ARTICLE

Automated projection spectroscopy in solid-state NMR

Alexander Klein[1,2] · Suresh K. Vasa[1,2] · Rasmus Linser[1,2,3]

Abstract

Given that solid-state NMR is being used for protein samples of increasing molecular weight and complexity, higher-dimensionality methods are likely to be more and more indispensable for unambiguous chemical shift assignments in the near future. In addition, solid-state NMR spectral properties are increasingly comparable with solution NMR, allowing adaptation of more sophisticated solution NMR strategies for the solid state in addition to the conventional methodology. Assessing first principles, here we demonstrate the application of automated projection spectroscopy for a micro-crystalline protein in the solid state.

Introduction

Solid-state NMR has been bestowed with manifold innovative possibilities and developments over the last years. One important achievement is the detection of protons as a routine approach for chemical shift assignments, structure calculation, as well as characterization of dynamics (Vasa et al. 2018b). Owing to an increase in sensitivity and the facilitated tailoring of multi-dimensional sequences effectively dispersing chemical shift degeneration, target proteins in solid-state NMR have become more and more demanding and complex (Quinn and Polenova 2017). Higher-dimensionality (dimensionality larger than 3) has played a role for novel solid-state NMR sequences only in recent years, facilitated by non-uniform sampling approaches (Hyberts et al. 2010, 2012; Hoch et al. 2014; Palmer et al. 2015) in four dimensions. As such, through-space correlations for structure elucidation (Huber et al. 2012; Linser et al. 2014; Shi et al. 2015) as well as backbone assignment experiments have been bestowed with four dimensions, enabling unambiguous assignment of increasingly large spin systems (Vasa et al. 2018b; Fraga et al. 2017; Zinke et al. 2017; Xiang et al. 2014, 2016). Prospectively, four dimensions will have an increasing likelihood to fail for solid proteins exceeding 50 kDa, however, due to increasing signal overlap as well as assignment ambiguities associated with the linewidths usually found for solid preparations. As such, higher-dimensionality techniques will be increasingly sought. Pulse sequences in which more than four nuclei could be encoded without additional transfer pathways are already up and (reliably) running, for example the HNcacoNH (Xiang et al. 2015), which we have used very successfully in four dimensions (Vasa et al. 2018b) and which has also been suggested on the basis of CC-INEPTs in 3D (Andreas et al. 2015).

Reconstructing higher-dimensionality spectra with more than four dimensions on the basis of non-uniform sampling (NUS) methods used in the solid state has so far been challenged by missing NMRpipe scripts as well as the increasing hardware and computation time requirements for reconstruction and data storage. One way of implementing multiple dimensions with a low burden of spectral reconstruction is the concept of projection reconstruction (PR) originally proposed by Kupce and Freeman (2004) or the related approach by Hiller and Wüthrich (automated projection spectroscopy, APSY), which relies on geometric analysis instead of full reconstruction of all the dimensions (Hiller et al. 2005, 2008b). Both methods trace back to the projection cross-section theorem proposed by Nagayama et al. (1978), which

✉ Rasmus Linser
  rasmus.linser@lmu.de

1 Department of Chemistry, Ludwig-Maximilians-University Munich, Butenandtstr. 5-13, 81377 Munich, Germany

2 Center for Integrated Protein Science (CiPSM), Munich, Germany

3 Faculty of Chemistry and Chemical Biology, Technical University Dortmund, Otto-Hahn-Straße 4a, 44227 Dortmund, Germany

states that a cross-section in the two-dimensional time–space running through the origin with an angle α (the time increment of one of the two indirect evolution periods being multiplied by cos α and the increment of the other one by sin α) Fourier-transforms into the corresponding projection in frequency space. PR methods determine those frequencies correlated in a higher-dimensionality experiment by a number of lower-dimensionality projections, normally 2Ds, of different orientations, which are obtained by simultaneous incrementation of the various indirect evolution periods in different ratios, while the direct acquisition dimension is constant. The orientation of the planes and thereby the ratio of the indirect dimensions A and B in a multidimensional space depends on the Euler angles and as such on the dimensionality of the original experiment (Kupce and Freeman 2004; Hiller et al. 2005; Nagayama et al. 1978). As all planes, except the orthogonal ones, run through two indirect dimensions simultaneously, each time increment requires multiple phase increments to obtain quadrature detection of the signal. In case of a 3D experiment, combining two phases required for each one of two evolution periods results in four differently modulated FIDs S_1–S_4.

$$S_1 = \cos(\Omega_A t \cos\alpha)\cos(\Omega_B t \sin\alpha) \tag{1}$$

$$S_2 = \cos(\Omega_A t \cos\alpha)\sin(\Omega_B t \sin\alpha) \tag{2}$$

$$S_3 = \sin(\Omega_A t \cos\alpha)\cos(\Omega_B t \sin\alpha) \tag{3}$$

$$S_4 = \sin(\Omega_A t \cos\alpha)\sin(\Omega_B t \sin\alpha) \tag{4}$$

(For experiments with higher dimensionality the number of phase combinations required is doubled for each additional dimension.) The sums and differences of these FIDs, i.e. the combinations S_1–S_4 and S_2+S_3, as well as S_1+S_4 and S_2–S_3, can then be Fourier-transformed into projection spectra as a set of the +α and the −α plane (Kupce and Freeman 2004).

In APSY, after peak picking in such spectra, a list containing all potential (but not necessarily existent) underlying shift combinations that would give rise to the projections obtained is created from a subset of these and then verified by successively taking into account additional projections. A peak in the reconstructed multi-dimensional space is considered to be real when a certain parameter called "support", which is the count of projections that do support the candidate peak to be real, is above a certain threshold. For more details see works by Hiller et al. (2005, 2008b). The final list of verified multi-dimensional shift combinations can then be used by automated backbone assignment routines like MARS (Jung and Zweckstetter 2004), CYANA/FLYA (Schmidt and Güntert 2012), UNIO/MATCH (Volk et al. 2008) or GARANT (Bartels et al. 1996; Christian et al. 1997), which has been demonstrated both for backbone and

sidechains (Volk et al. 2008; Krähenbühl et al. 2013; Fiorito et al. 2006; Gossert et al. 2011; Hiller et al. 2008a). In solution, APSY has been successfully applied for proteins up to 38 kDa using deuteration and TROSY approaches (Krähenbühl et al. 2013).

Whereas sharp line widths are normally obtained in liquid-state NMR for small or medium-sized proteins due to motional averaging, solid-state NMR generally suffers from broader homogeneous line widths. In addition, sample heterogeneity can increase both line widths and signal overlap. Unfortunately, the effective line width in tilted projections is always broader compared to conventional or orthogonal projections (Kupce and Freeman 2004). Therefore, the application of APSY in the solid state seems not obvious. Here we show that projection reconstruction is possible for solid-state NMR, even though peak widths are larger than for most solution NMR spectra. On this basis, a range of possible solid-state NMR strategies emerge that may aid solving upcoming challenges brought upon by future solid-state NMR targets.

Experimental

All NMR spectra were recorded on a micro-crystalline sample of the SH3 domain of deuterated and 100% exchangeable-proton back-exchanged chicken α-spectrin, recombinantly produced using $^{13}C_6$, $^2H_7$-glucose, $^{15}NH_4Cl$, and D_2O and doped with 75 mM Cu-edta as described conceptually previously (Linser et al. 2007). After filling the sample into a 1.3 mm rotor with fluorinated rubber plugs NMR spectra were recorded at a rotor frequency of 50 kHz MAS at approximately 15 °C effective temperature on a Bruker NEO spectrometer with a proton Larmor frequency of 700 MHz. Under such conditions, assuming sufficient duration of evolution periods, the SH3 domain sample provides linewidths on the order of 40–100 Hz for protons and around 15–20 Hz for nitrogens. All magnetization transfers were enabled by dipolar methods (CP (Hartmann and Hahn 1962) and BSH-CP (Chevelkov et al. 2013) for heteronuclear and homonuclear transfers, respectively), with settings similar as described earlier (Vasa et al. 2018a). All experiments were acquired with 12 different values for the angle α as shown in Table 1, each α being associated with a +α and a −α projection. Including the two orthogonal planes, this results in sets of 22 spectra for each experiment.

As each recording of a plane involves four FIDs per time increment to enable quadrature detection in the two indirect evolution periods, the number of increments in the (single) indirect dimension present has to be chosen twice as high as desired in an individual dimension of a 3D experiment. In accordance with each plane being acquired with 320 indirect and 2048 direct points set, 80 time increments were obtained.

Table 1 List of angles α used for APSY on micro-crystalline SH3

α in °	# of angles	Spectra per angle
0	1	1
90	1	1
38.9, 58.2, 21.9, 72.8, 11.4, 81.2, 5.8, 50.4, 28.2, 45.0	10	2

For each non-orthogonal angle two sets of spectra are obtained, corresponding to the plane with an angle $\pm\alpha$. The angles were chosen to be equally distributed between 0° and 90°

Indirect-dimension time increments in the hCONH, hCANH, hCOcaNH and hCAcoNH were 280, 200, 180 and 200 µs, respectively, for ^{13}C and 360 µs for ^{15}N, resulting in a spectral width of 20.2 ppm, 28.3 ppm, 31.5 ppm, 28.3 ppm and 39.1 ppm, respectively. This results in a t_{1max} of 23 ms, 16 ms, 14 ms, 16 ms and 29 ms, respectively, as of the maximal-incrementation case obtained in orthogonal planes. The 3D-hCANH and hCONH were acquired with 8 scans, while the 3D-hCAcoNH/hCOcaNH pair was acquired with 16 scans for each FID—resulting in an experimental time of 37 min, 38 min, 61 min, and 73 min, respectively, for any non-orthogonal pair of angles of the four experiments. In the orthogonal projection planes the number of scans was halved compared to the non-orthogonal planes (half experimental time). This yields a total experimental time of 13.3 h for the hCONH, 13 h for the hCANH, 25.5 h for the hCOcaNH and 21.4 h for the hCAcoNH experiment.

APSY acquisition was done by a TopSpin macro (kindly provided by Sebastian Hiller), which controls the projection angles setup and acquisition of the corresponding projections. The 3D pulse programs for APSY were modified according to TopSpin 2.X. After acquisition of all the planes, we used a simple self-written TopSpin macro to sort and recombine the acquired FIDs in such a way that projections are obtained in quadrature mode (See Eqs. 1–4). These modified FIDs were processed by standard 2D processing tools in TopSpin. All the subsequent steps, i.e. peak picking and geometric analysis of peak positions, are done by APSY-related scripts (including GAPRO for geometric analysis) that were kindly provided by Sebastian Hiller. These do not run in TopSpin and are used via the command line in Linux. The actual analysis, i.e. peak picking and analysis of peak positions, runs in less than one minute on modern notebooks.

Results

We reconstructed a set of 3-dimensional experiments required for backbone assignment of proteins, namely (CP-based) hCANH and hCONH (Zhou et al. 2007), as well as

fully dipolar hCOcaNH and hCAcoNH (Xiang et al. 2016) experiments, on the basis of 2-dimensional H(N/C) projections. The established pulse sequences were modified for the existing APSY routine (Hiller et al. 2005) by implementing two sorts of changes to standard solid-state NMR sequences. On one hand, the pulse sequence header required for automation of projection angle determination was added to the sequence. On the other, the acquisition loops were adapted for four phases for each time increment for all non-0° and non-90° planes to obtain States quadrature detection in both indirect dimensions. As such, all increments were recorded using phase-sensitive incrementation by 90° shifts of each CP spin lock before any of the indirect time evolutions, consequently yielding four FIDs per time increment. Processing to complex projection spectra at $\pm\alpha$ angles was achieved as described by Kupce and Freeman (2004), by simple addition and subtraction of the individual FIDs and sorting the resulting FIDs into separate data sets for plus and minus angles.

Figure 1 exemplifies the orientation of different planes in three-dimensional frequency space. The orthogonal planes, i. e. projections with $\alpha=0°$ or $\alpha=90°$, correspond to projections of the F3/F2 and F3/F1 planes in a conventional experiment and therefore should look the same compared with conventional projections (or conventional 2D spectra). The front plane ($\alpha=0°$) displays the NH plane with ^{1}H as the direct dimension. The top plane ($\alpha=90°$) corresponds to the H/C$^\alpha$ plane. Both projections share the direct dimension.

The signals visible in non-orthogonal projections (Fig. 1 right) consist of a mixture of the individual heteronuclear frequencies, such that their chemical shift in the indirect dimension depends on the angle α, as it is reflected in Eqs. 1–4. As the GAPRO algorithm performs a geometric reconstruction of peak positions, a plain peak list is the output. Figure 2 displays the overlaid HN shift correlations from peak lists reconstructed for the different 3D experiments employed in this work after GAPRO analysis. The HN peaks group well, indicating that the reconstruction performs reliably for different experiments in terms of chemical-shift accuracy. The number of peaks obtained, however, slightly differs among the four experiments for different reasons: on one hand, different numbers of peaks are indeed expected from the kind of experiment. E.g., the H/N correlations of arginine and glutamine side chains are not visible in hCANH and hCOcaNH but show up in hCONH and hCAcoNH. On the other hand, however, reconstruction success is dependent on the separation of peaks in the various projections (see below). Figure 2b gives examples for residues in crowded regions as well as for weak peaks that are not found in APSY although they are detectable in the conventional 3D experiment.

Table 2 shows the number of peaks that were reconstructed by APSY in comparison to a dataset of experiments acquired conventionally. For all experiments $\geq 90\%$ of the
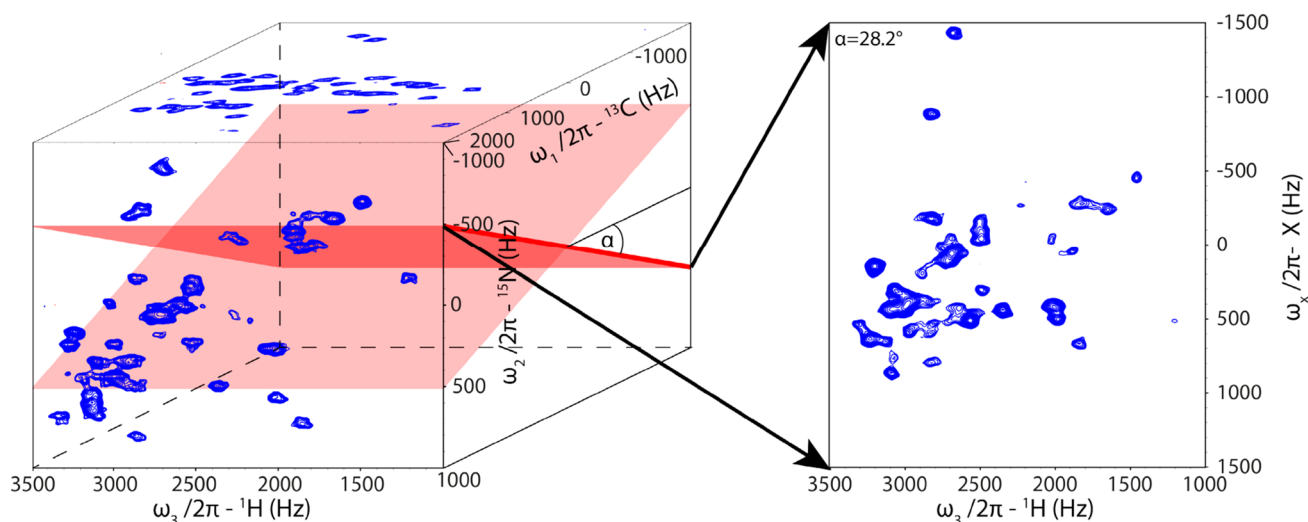
Fig. 1 Exemplary representation of projection planes. Shown in blue are the α=0° and α=90° planes, representing the HN and the HCᵅ projections, and indicated in red are the ± projections of an arbitrary angle 0° < α < 90°. One such projection is depicted on the right. All axes are shown in the frequency domain, 0 Hz representing the carrier frequency, rather than in ppm
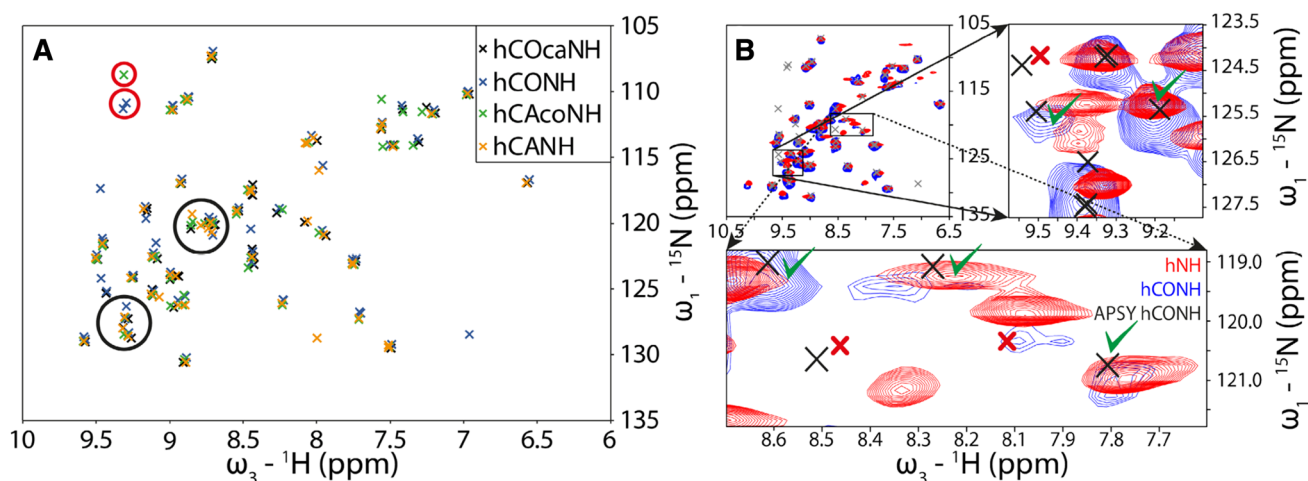

Fig. 2 **a** Overlay of H/N correlations from predicted peak positions of all acquired experiments after GAPRO analysis. The number of peaks varies among the experiments for different reasons. (See the text.) The peak positions, however, show reasonably high precision (average deviations of 0.005 ppm and 0.03 ppm for ¹H and ¹⁵N, respectively). Highlighted by red circles are artifact peaks (peaks not showing up in the conventional 3D experiment). Black circles highlight examples for crowded regions that lead to difficulties for correct shift determination. **b** Overlay of 2D H/N projection of a conventional hCONH experiment (blue) and a 2D hNH experiment (red) with the corresponding APSY hCONH peaks (black crosses). In the zoomed spectral regions, correct analysis of the peak positions is more challenging due to spectral crowding or inefficient magnetization transfers

peaks could be reconstructed. The missing peaks are located in overlapping regions or are derived from residues particularly affected by multiple magnetization transfer. As can also be seen in Fig. 2 (peaks outside groups of crosses), a small number of peaks can be considered as artifacts. Among all peaks in all experiments their relative number is small (ca. 2.5%).

For isolated peaks, where the belonging of each peak is clear, we calculated the average deviation among the

Table 2 An overview of the total number of peaks reconstructed by APSY in comparison with conventional experiments

	hCANH	hCAcoNH	hCONH	hCOcaNH
APSY	50	52	61	51
Conventional	53	58	66	51
Fraction	94%	90%	92%	100%

Although on average 6% of the peaks expected are missing, APSY generally detects peaks correctly in the solid-state NMR context. The missing peaks can be considered as overlapping or weak

different experiments to determine the precision of the analysis. As already indicated visually in Fig. 2a the precision among different experiments is generally high, which is an important prerequisite for automated assignment. The average deviation among reconstructed shift values belonging to the same peak over all isolated peaks in the H/N projections and all acquired experiments is 0.005 ppm for the ^{1}H dimension and 0.03 ppm for the ^{15}N dimension, i.e., below the FID resolution in both cases. Whereas both dimensions show high precision for isolated and well-defined peaks, for peaks in more problematic crowded regions a deviation cannot be defined as it is not clear which actual peak a reconstructed shift belongs to.

As described in the "Experimental" section the hCANH experiment (22 2D planes) was recorded in ca. 12.5 h initially. A conventional 3D experiment with the same maximum incrementation (t_{1max} of 29 ms and 16 ms in the ^{15}N and ^{13}C dimension, respectively) would require ca. 78 h, however, in praxis not so many increments would necessarily be acquired (see below). We are comparing experiments with a comparable number of scans, since the experimental-time considerations are most sensible with respect to the resolution-limited regime. The number of projections necessary depends on several factors, including sensitivity and number of expected peaks (Hiller et al. 2008; Hiller and Wider 2012). As such, no general rule can be provided. In solution, 5D APSY experiments have successfully been recorded with 18 different 2D projections (Hiller et al. 2008; Hiller and Wider 2012). Therefore, we assumed that no more than 20 projections (plus 2 orthogonal planes) should be required for 3D spectra with on the order of 55 expected peaks. To find out how much further we could decrease the APSY recording time, we reduced—exemplarily for the hCANH—the number of projections used for reconstruction in a stepwise manner. The number of peaks found for the initial set of 22 projections was used as reference. These results are summed up in Table 3.

As shown in Table 3, the number of projections in our 55-residues case can be reduced to ten non-orthogonal (plus two orthogonal) planes with only a slight effect on the number of identified peaks. (For less than ten non-orthogonal planes the results obtained were no longer reasonable.) For isolated and well-defined peaks, the reconstruction is still robust and accurate, as indicated by the RMSDs (chemical-shift deviation from the reference peak position in conventional data) for all dimensions (Table 3, bottom). These are on the order of the FID resolution and do not significantly vary between the different sets of projection planes. There are, however, some peaks whose reconstruction success does vary between conditions. These peaks represent the broad and weak ones in the conventional data set or such that suffer from overlap. In the case of 16 non-orthogonal projections more peaks than in the reference are found. The case of

Table 3 Completeness of reconstructed peaks in the hCANH experiment for different numbers of projection planes employed

Number of planes	20 + 2	16 + 2	10 + 2	Conventional 3D
Peaks found	50	57	46	53
(GAPRO parameters:)				
$S_{min1,2}$[a]	7	7	7	
r_{min}[b]	50.0 Hz	40.0 Hz	55.0 Hz	
$\Delta\nu$[c]	20.0 Hz	18.0 Hz	25.0 Hz	
RMSD[d] ^{1}H/ppm	0.034	0.033	0.036	
RMSD[d] ^{15}N/ppm	0.17	0.15	0.18	
RMSD[d] ^{13}C/ppm	0.18	0.19	0.19	

For more details on the parameters see Hiller et al. (2005, 2008b) and Hiller and Wider (2012)

[a]$S_{min1,2}$: minimal support needed for a peak candidate

[b]r_{min}: peak matching tolerance in the indirect dimension

[c]$\Delta\nu$: peak matching tolerance in the direct dimension

[d]Conventional 3D as reference for RMSD calculation

reducing projections reveals the problem of reconstructing peaks in strongly overlapping regions and broad peaks.

This difficulty can also be seen in Fig. 3, which shows the overlaid H/N (left) and H/C$^\alpha$ peak positions for the different completeness levels of hCANH input data in a pictorial way. Thus, it is possible to get reasonable results (accurate reconstruction) of the more unproblematic peaks even with less projections. In most cases, however, this comes hand in hand with an increased number of artifact peaks. Therefore, a high number of projections is indeed better in resolving overlapping regions and eradicating false peaks. The high accuracy is nicely represented by cross overlap in Fig. 3.

To obtain the best agreement with the untruncated data set, we had to slightly optimize the GAPRO parameters in each case, as is listed in the lower part of Table 3. Reasonable starting values for the parameters r_{min} and $\Delta\nu$ correspond to the FID resolution in the indirect and direct dimension. The starting value for the support parameter $S_{min1,2}$ can be set to the dimensionality of the experiment, as it is recommended by the APSY program suite. As one can see from Table 3, however, the optimal support is significantly higher in our case. This indicates that for our conditions, noise and most artifacts are very well distinguished from actual peaks. However, one will find an increased number of artifacts when the support is set too low, or, conversely, the number of correct peaks will drop when the support is set too high. In the minimal-data case, the number of used projection planes and the support has increased from ca. 30% to over 50%. Therefore, it seems helpful to set the support and the matching tolerance high enough, as artifacts can be hard to distinguish from correct peaks, at least without a reference. (Usually, a reference 2D spectrum does exist.) In any case, when complementary experiments are
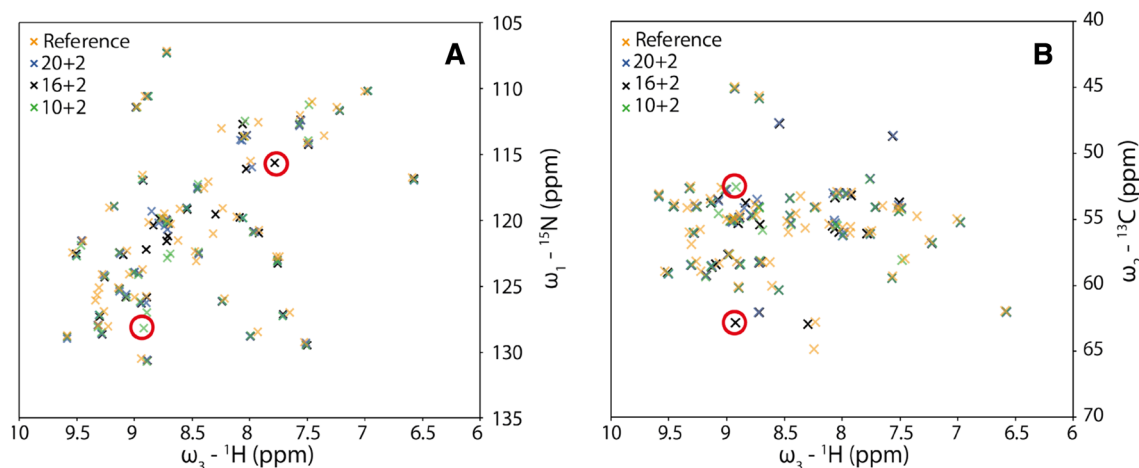
Fig. 3 Comparison of reconstruction success for various levels of data completeness. The plots show **a** the shifts in the H/N plane and **b** in the H/C plane of a test hCANH experiment. Shifts are represented in orange (reference spectrum), blue (20 non-orthogonal projection planes), black (16 non-orthogonal projection planes), and green (10 non-orthogonal projection planes). Highlighted with red circles are artifacts that are found for different numbers of projections (see text). The accuracy and precision of peak positions remains high (see Table 3)

acquired, artifacts can be identified as peaks that appear only in one spectrum. As in solution, similar problems may occur for other GAPRO parameters as described in detail by Hiller et al. (2008b) and Hiller and Wider (2012).

Compared to the whole set with 20 non-orthogonal planes, the 10 + 2 set corresponds to an additional time saving of slightly less than a factor of two, as such resulting in an overall saving of 12 compared to the conventional experiment. In case the conventional 3D experiments were not acquired with such a high resolution and therefore long acquisition times (Under the conditions of this study, a more reasonable experimental time of 30 h would correspond to 60 time increments in the ^{15}N dimension and 40 time increments in the ^{13}C dimension.), using APSY is still 2.5 times faster in spite of a significantly increased resolution. Again considering the hCANH, but now reducing the resolution of each indirect dimension by half (to 40 time increments corresponding to indirect acquisition times t_{1max} of 14.4 ms and 8 ms for ^{15}N and ^{13}C respectively), we find no changes neither in the number of reconstructed peaks nor in their positions. This would allow to record the set of 22 spectra, i.e. 20 non-orthogonal planes plus two orthogonal ones, in less than 8 h. Furthermore, GAPRO directly performs a peak picking and therefore manual and time-consuming peak picking may save time in more complicated data sets.

Discussion

The APSY method offers some advantages over other techniques like Hadamard spectroscopy (Kupce et al. 2003) or NUS in the solid state. On the one hand, it does not require any kind of knowledge about the overall form of the spectrum, like regions without peaks. On the other hand, conventional FT-based processing routines can be used. There is no need for specialized NMRpipe scripts etc., however, the pulse program changes and processing features described need to be implemented. The underlying GAPRO algorithm for creating the multidimensional peak list completes in < 1 min on modern computers, whereas e.g. NUS reconstruction by IST (Hyberts et al. 2012) requires significantly more computation time for a comparable dataset on a conventional PC. Therefore, it is relatively easy and fast to optimize processing and GAPRO parameters for the projection planes of the underlying chemical shifts. Recombining the acquired FIDs to obtain ± angles in quadrature mode is currently the most time-consuming step of processing in our hands, which will be more pronounced when processing 4D, 5D, or 6D spectra. As APSY creates only peak lists and no generation of spectra is performed, APSY is predestined for the use of automated (backbone) assignment routines, in particular for high dimensionalities.

APSY can provide a significant saving of acquisition time already for low dimensional experiments. In general, the maximum time saving factor (for a 3D experiment) is

$$F = \frac{t_{3D}}{t_{APSY} \cdot 2(n+1)} \tag{5}$$

where $2(n+1)$ corresponds to the number of individual projection planes with experimental time t_{APSY} each, obtained from n number of (positive) α values, and t_{3D} corresponds to the experimental time of the conventional 3D experiment.

The overall time saving, therefore, strongly depends on the number of acquired planes and the acquisition time in each of the indirect dimensions. As such, a specific factor for time saving depends on the requirements of the sample, and the number of projections has to be set individually. On the other hand, high resolution is achieved at a relatively lower cost than in conventional data acquisition. In theory, time savings of one order of magnitude can be easily obtained for three dimensions in the resolution-limited regime. This effect will be more pronounced when increasing the number of dimensions.

A major drawback of the (2D projection-based) APSY method is that the algorithm becomes less reliable when peak overlapping in any two-dimensional projections occurs. Obviously, however, such residues are also the ones where conventional experiments will have their shortcomings, and manual assignment will equally require complementary or higher-dimensionality experiments. Also for APSY, one can avoid this problem by using higher-dimensionality experiments, as demonstrated for liquid-state NMR spectroscopy. Similarly, like for conventional spectroscopy, resolution problems can be further reduced in combination with specific labeling schemes (Krähenbühl et al. 2013; Gossert et al. 2011). Generally speaking, well-resolved projection planes are required. Solid-state NMR tends to be associated with homogeneous and inhomogeneous line broadening, which exacerbates exactly this potential problem of overlapping peaks. On the other hand, owing to efficient magnetization transfers irrespective of tumbling correlation times, the design of higher-dimensionality experiments has been shown to be facilitated (Vasa et al. 2018a; Fraga et al. 2017; Zinke et al. 2017). This is particularly important as APSY will rather suffer from low sensitivity than from overlap when using higher-dimensionality experiments (Hiller et al. 2005). As such, APSY may represent an additional, valuable asset for many proteins of large effective molecular weight. By contrast, for inhomogeneous sample preparations, which can be tackled by conventional higher-dimensionality spectroscopy (Xiang et al. 2016) but for which proton line widths in the direct dimension are broad, it seems that APSY will remain challenging.

APSY does not analyze the intensity information or the contours of line shapes. For those cases it may be beneficial to use other sparse sampling methods, which each have their individual benefits and drawbacks, however. A general rule when to use which technique is difficult to set and strongly depends on the scope of the experiment as well as requirements. Nevertheless, APSY is one of those alternatives also for solid-state NMR and might offer the biggest time savings in particular for dimensions ≥ 3 if only chemical shifts are of interest. For a more detailed analysis of the several methods the authors would like to refer to (solution NMR) literature by Kazimerczuk et al. (2010) and Nowakowski et al. (2015).

Besides the principle applicability of projection reconstruction for solid-state NMR demonstrated here, a vast space of far more complex experiments will open up by combination of methodology. The real advantages will come to play for the various higher-dimensionality experiments, which often no conventional alternative exists for to-date.

In conclusion, we have demonstrated the use of Automated Projection Spectroscopy (APSY) for solid-state NMR using proton-detected backbone assignment experiments on a small micro-crystalline protein. Despite the larger line widths in the solid state, APSY works reliably for most peaks and represents a viable direction for computer-aided signal assignment complementary to manual approaches. However, crowded regions cannot always be faithfully reconstructed even with high numbers of projection angles. Given that solid-state NMR spectra do have a higher tendency for peak overlap, higher-dimensional APSY spectra than used here will be required already for lower-molecular-weight proteins than for solution NMR APSY. Nevertheless, we think that APSY will be a complementary tool for those systems in solid state NMR that require higher-dimensionality spectra due to spin system complexity. Even when using three-dimensional experiments, APSY offers a significant time saving and a suitable output for automatic assignment strategies. For higher dimensionality, it will thus represent a viable one out of a limited number of alternatives.

Compliance with ethical standards

Conflict of interest The authors declare no competing financial interests.

References

Andreas LB et al (2015) Protein residue linking in a single spectrum for magic-angle spinning NMR assignment. J Biomol NMR 62:253–261

Bartels C, Billeter M, Güntert P, Wüthrich K (1996) Automated sequence-specific NMR assignment of homologous proteins using the program GARANT. J Biomol NMR 7:207–213

Chevelkov V, Giller K, Becker S, Lange A, Efficient (2013) CO-CA transfer in highly deuterated proteins by band-selective homonuclear cross-polarization. J Magn Reson 230:205–211

Christian B, Peter G, Martin B, Kurt W (1997) GARANT-a general algorithm for resonance assignment of multidimensional nuclear magnetic resonance spectra. J Comput Chem 18:139–149

Fiorito F, Hiller S, Wider G, Wüthrich K (2006) Automated resonance assignment of proteins: 6 DAPSY-NMR. J Biomol NMR 35:27–37

Fraga H et al (2017) Solid-state NMR H–N–(C)–H and H–N–C–C 3D/4D correlation experiments for resonance assignment of large proteins. ChemPhysChem 18:2697–2703

Gossert AD, Hiller S, Fernández C (2011) Automated NMR resonance assignment of large proteins for protein-ligand interaction studies. J Am Chem Soc 133:210–213

Hartmann SR, Hahn EL (1962) Nuclear double resonance in the rotating frame. Phys Rev 128:2042–2053

Hiller S, Wider G (2012) Automated projection spectroscopy and its applications. Top Curr Chem 316:21–48

Hiller S, Fiorito F, Wüthrich K, Wider G (2005) Automated projection spectroscopy (APSY). Proc Natl Acad Sci USA 102:10876–10881

Hiller S, Joss R, Wider G (2008a) Automated NMR assignment of protein side chain resonances using automated projection spectroscopy (APSY). J Am Chem Soc 130:12073–12079

Hiller S, Wider G, Wüthrich K (2008b) APSY-NMR with proteins: practical aspects and backbone assignment. J Biomol NMR 42:179–195

Hoch JC, Maciejewski MW, Mobli M, Schuyler AD, Stern AS (2014) Nonuniform sampling and maximum entropy reconstruction in multidimensional NMR. Acc Chem Res 47:708–717

Huber M, Böckmann A, Hiller S, Meier BH (2012) 4D solid-state NMR for protein structure determination. Phys Chem Chem Phys 14:5239–5246

Hyberts SG, Takeuchi K, Wagner G (2010) Poisson-gap sampling and forward maximum entropy reconstruction for enhancing the resolution and sensitivity of protein NMR data. J Am Chem Soc 132:2145–2147

Hyberts SG, Milbradt AG, Wagner AB, Arthanari H, Wagner G (2012) Application of iterative soft thresholding for fast reconstruction of NMR data non-uniformly sampled with multidimensional poisson gap scheduling. J Biomol NMR 52:315–327

Jung Y-S, Zweckstetter M (2004) Mars—robust automatic backbone assignment of proteins. J Biomol NMR 30:11–23

Kazimierczuk K, Stanek J, Zawadzka-Kazimierczuk A, Kozminski W (2010) Random sampling in multidimensional NMR spectroscopy. Prog Nucl Magn Reson Spectrosc 57:420–434

Krähenbühl B, Boudet J, Wider G (2013) 4D experiments measured with APSY for automated backbone resonance assignments of large proteins. J Biomol NMR 56:149–154

Kupce E, Freeman R (2004) Projection-reconstruction technique for speeding up multidimensional NMR spectroscopy. J Am Chem Soc 126:6429–6440

Kupce E, Nishida T, Freeman R (2003) Hadmard NMR spectroscopy. Prog Nucl Magn Reson Spectrosc 42:95–122

Linser R, Chevelkov V, Diehl A, Reif B (2007) Sensitivity enhancement using paramagnetic relaxation in MAS solid-state NMR of perdeuterated proteins. J Magn Reson 189:209–216

Linser R et al (2014) Solid-state NMR structure determination from diagonal-compensated, sparsely nonuniform-sampled 4D proton–proton restraints. J Am Chem Soc 136:11002–11010

Nagayama K, Bachmann P, Wüthrich K, Ernst RR (1978) The use of cross-sections and projections in two-dimensional NMR spectroscopy. J Magn Reson 31:133–148

Nowakowski M, Saxena S, Stanek J, Zerko S, Kozminski W (2015) Applications of high dimensionality experiments to biomolecular NMR. Prog Nucl Magn Reson Spectrosc 90–91:49–73

Palmer MR et al (2015) Sensitivity of nonuniform sampling NMR. J Phys Chem B 119:6502–6515

Quinn CM, Polenova T (2017) Structural biology of supramolecular assemblies by magic-angle spinning NMR spectroscopy. Q Rev Biophys 50:e1

Schmidt E, Güntert P (2012) A new algorithm for reliable and general NMR resonance assignment. J Am Chem Soc 134:12817–12829

Shi C et al (2015) Atomic-resolution structure of cytoskeletal bactofilin by solid-state NMR. Sci Adv 1:e1501087

Vasa SK, Singh H, Rovó P, Linser R (2018a) Dynamics and interactions of a 29-kDa human enzyme studied by solid-state NMR. J Phys Chem Lett 9:1307–1311

Vasa SK, Rovó P, Linser R (2018b) Protons as versatile reporters in solid-state NMR spectroscopy. Acc Chem Res 51:1386–1395

Volk J, Herrmann T, Wüthrich K (2008) Automated sequence-specific protein NMR assignment using the memetic algorithm MATCH. J Biomol NMR 41:127

Xiang S, Chevelkov V, Becker S, Lange A (2014) Towards automatic protein backbone assignment using proton-detected 4D solid-state NMR data. J Biomol NMR 60:85–90

Xiang S et al (2015) Sequential backbone assignment based on dipolar amide-to-amide correlation experiments. J Biomol NMR 62:303–311

Xiang S, Biernat J, Mandelkow E, Becker S, Linser R (2016) Backbone assignment for minimal protein amounts of low structural homogeneity in the absence of deuteration. Chem Commun 52:4002–4005

Zhou DH et al (2007) Solid-state protein structure determination with proton-detected triple resonance 3D magic-angle spinning NMR spectroscopy. Angew Chem Int Ed 46:8380–8383

Zinke M et al (2017) Bacteriophage tail tube assembly studied by proton-detected 4D solid-state NMR. Angew Chem Int Ed 129:9625–9629